AUT Journal of Electrical Engineering
10.22060/EEJ.2026.25286.5894

Advanced Power Quality Improvement Using Re-Lift Sepic Converter and DSTATCOM with Neural Network Control

S. Ramachandran[1]*, K. Sakthidhasan[2], M. Pandikumar[3], L. Anbarasu[4]

[1]Assistant Professor, Department of Electrical and Electronics Engineering, Paavai Engineering College, Namakkal, Tamil Nadu, India.

[2]Assistant Professor, Department of Electrical and Electronics Engineering, Vel Tech Multi Tech Dr. Rangarajan Dr. Sakunthala Engineering College, Chennai-600062, Tamil Nadu, India.

[3]Associate Professor, Department of Electrical Power and Energy Conversion, Saveetha School of Engineering, SIMATS, Chennai-602105, Tamil Nadu, India

[4]Associate Professor, Department of Electrical and Electronics Engineering, Erode Sengunthar Engineering College Perundurai, Erode-638057, Tamil Nadu, India.

*Corresponding author E-mail: contacttoramachandran@gmail.com

Abstract:

At present power system faces certain Power Quality (PQ) issues, due to large amount of power usage, fluctuations and other uncertainties in non-linear loads. Thus, Distribution Static Compensator (DSTATCOM) is deployed for mitigating PQ problems. A three-phase AC source system, supplying a non-linear load using parallel-Voltage Source Inverter (VSI) based DSTATCOM at Point of Common Coupling (PCC) is deployed to DC-Link which functions based on current sharing principle. A novel Re-lift Single Ended Primary Inductor Converter (SEPIC) converter is integrated with Photovoltaic (PV) to boost PV power generation, assuring consistent and sustainable power supply to DC-Link capacitor of DSTATCOM is correctly charged. To further enhance the system performance, D-Q theory/Neural Network-based Synchronous Reference Frame (SRF) theory is utilized for generating reference current for DSTATCOM. These control topologies enable accurate compensation of reactive power and harmonic currents in real-time, assuring improved grid voltage stability and rectifying distortions. Proposed system is executed using MATLAB simulation and acquired outcomes validate improved system functioning with better PQ mitigation at PCC under varying load conditions. Thus, demonstrating the impacts of integrating renewable energy with advanced control approaches.

AUT Journal of Electrical Engineering
10.22060/EEJ.2026.25286.5894

Keywords:

PQ issues, DSTATCOM, PCC, VSI, PV, Re-lift SEPIC, D-Q theory, SRF.

1. Introduction

The consistent expansion of distribution devices and non-linear loads are deforming the quality of power in distribution systems [1]. These PQ issues in any distribution system causes serious impacts that need to be rectified by keeping numerous parameters like greater load capability, usage of many power-driven equipment, zero voltage regulation [2].

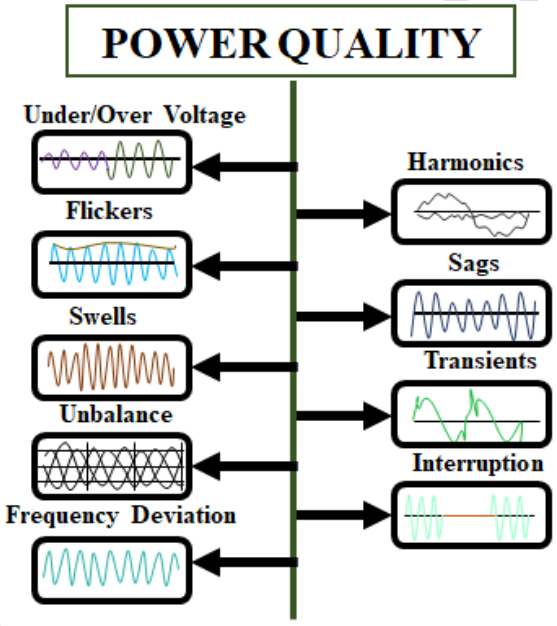

Fig. 1. Various PQ Issues

PQ issues as displays in Fig.1 are divided on the basis of voltage and current quality disputes [3]. Thus, various PQ enhancement approaches including Distributed Voltage Regulator (DVR) [4], Unified Power Quality Conditioner (UPQC) [5], Unified Power Flow Controller (UPFC) [6], Distributed Power Factor Controller (DPFC) [7] and Static Synchronous Compensator (STATCOM) [8] are considered for enhancing the overall PQ and system stability. More specifically, these approaches are developed to nullify the PQ

issues like voltage sags, swells, harmonics and imbalances, while also enhancing the power factor, regulating voltage levels , thus ensuring consistent and reliable performance of power distribution system [9]. But these approaches still cannot meet the desired level of performance, to be particular, despite these advantages, [10] DVR struggles with managing severe voltage sags under highly varying load conditions and also it not capable of identifying PQ issues and harmonics in a complex distribution system. [11] UPQC also struggles with similar limitations such as inability to handle severe voltage sags under varying load circumstances and load imbalances. Significantly, [12] UPFC requires high implementation cost making economically infeasible, moreover UPFC performance highly depends on power electronic devices which leads to increased losses, reduced efficiency and reliability. Similarly, [13] DPFC also depends upon power electronic devices, which also leads to increased losses with increased system sensitivity towards harmonic distortions, thereby, minimizing the PQ within the power systems. Lastly, [14] STATCOM consisting of many advantages still faces difficulties in controlling the power flow and its performance is restrained due to increased voltage sag conditions. Acknowledging these shortcomings, DSTATCOM based PQ enhancement approach is developed which depicts improved harmonics reduction even under varying load scenarios with compact and less maintenance, cost efficient and highly reliable for enhancing the power factor, thus, leading to improved system stability and reliability in mitigating the PQ issues. Furthermore, appropriate control techniques are important for ensuring the performance effectiveness of DSTATCOM, as they provide better power regulation and reference current generation. Therefore, various control approaches like Fuzzy Proportional Integral (PI) controller [15], Fuzzy Logic Controller (FLC) [16] and Deep Deterministic Policy Gradient (DDPG) [17] are regarded. These control approaches provide various benefits including improved dynamic responses, stability with better harmonics reduction. To be specific, Fuzzy PI controller integrates advantages of both fuzzy and PI controller ensuring improved system performance dynamic system conditions. FLC provides enhanced control by handling system uncertainties, suitable for complex system structures. Significantly, DDPG provides highly improved performance in terms of removing unwanted disturbances and interference, ensuring faster system responses. However,

these control topologies lack certain abilities, to particularize, Fuzzy PI struggles with tuning problems, FLC frequently requires additional computational resources and DDPG highly relies on parameter computation. Thus, D-Q theory/NN-based SRF theory is utilized which enables improved performance by generating reference current. The integration of D-Q theory/NN-based SRF theory improves the PQ with much faster responses with increased reliability and system stability. To further provide reliable and sustainable power supply to DC-Link PV system is deployed and to boost the PV power production, power converter play a major part. Conventional power converters including Re-Lift Luo [18] and Super-Lift Luo converter [19], where in spite the merits such as high voltage gain, improved efficiency, these converters also suffers increased complexity due to higher component requirement and voltage stress, therefore, Re-lift SEPIC converter is deployed which achieves highly regulated PV power output with increased voltage gain and stability. Therefore, the proposed system provides highly effective system performance with improved PQ rectification and reduced harmonics, assuring improved stability and reliability. Distinction of the proposed with existing literature as illustrates in Table 1.

Table 1. Distinction of proposed method from existing literature

Feature	Existing Works	Proposed work
NN usage	Standalone or PI assisted	Embedded in SRF loop
DC link Support	Grid-dependent	PV fed Re-Lift SEPIC
Converter role	Power boosting only	DC-link Stabilization
Dynamic loss estimation	Not considered	NN based Adaptive
THD (%)	>0.9	0.62

Contributions of developed system is given in the following,

- To improve and mitigate the PQ issues within the power distribution system using DSTATCOM, which assures improved rectification of power losses and harmonics.
- A DQ/NN-based SRF hybrid control technique is proposed, in which the neural network is incorporated within the SRF framework to adaptively estimate DC-link power losses and reference current, rather than serving as a standalone controller.
- Unlike previous NN-controlled DSTATCOM techniques that depend entirely on grid-side power, the proposed system actively supports the DC-link utilizing a PV-fed Re-Lift SEPIC converter, ensuring continuous compensating capabilities under dynamic load conditions.
- To boost and regulate the PV power production, Re-Lift SEPIC is implemented which achieves increased voltage gain with reduced losses.
- The combined interaction of the PV source, Re-Lift SEPIC converter, and NN-SRF-controlled DSTATCOM results in improved harmonic suppression (THD = 0.62%) and near-unity power factor under various kinds of operating conditions.

2. Proposed Methodology

Fig. 2 represents the developed system using DSTATCOM for mitigating the PQ issues within the power distribution systems. Initially, the power from the Three Phase AC source that needs to be transmitted to load contains certain PQ issues. To rectify PQ issues, DSTATCOM is deployed at the PCC along with parallel VSI for conversion of DC to AC, The implementation of DSTATCOM improves and rectifies the PQ issues by reducing voltage sag, swell and harmonics. Furthermore, the VSI is aided with LC filter and a transformer for smooth and effective functioning.

10.22060/EEJ.2026.25286.5894

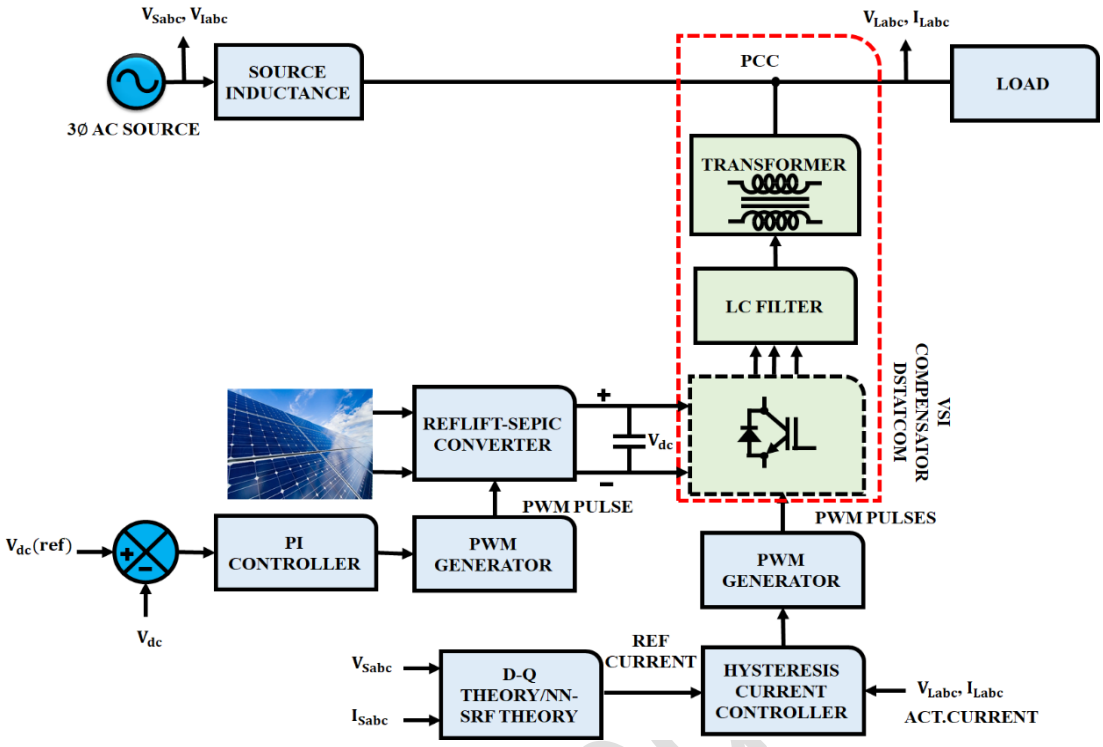

Fig. 2. Proposed System Block Diagram

Significantly, the DQ theory/NN-SRF theory is deployed for evaluating the three phase AC source voltages and the current for generating reference current for DSTATCOM. Then, obtained reference current is compared with actual load current using hysteresis current controller. Later, PV system is installed to the proposed to produce sufficient and sustainable power supply to the DC-link, additionally, Re-Lift SEPIC converter is connected to PV system for boosting PV power output thus, ensuring consistent charging of DC-Link. A PI controller is used regulate and control converter performance and a PWM generator is utilized for generating PWM pulses that drive the converter switching operation. Therefore, the development of advanced PQ enhancement system using DSTATCOM effectively provides sustainable and reliable performance with overall PQ improvement under varying load conditions.

2-1- Modelling of DSTATCOM

10.22060/EEJ.2026.25286.5894

D-STATCOM is a shunt device that introduces and consumes both reactive and active current. The D-STATCOM, PQ improvement component comprising of a VSI with a capacitor using a DC energy source is given in Fig. 3.

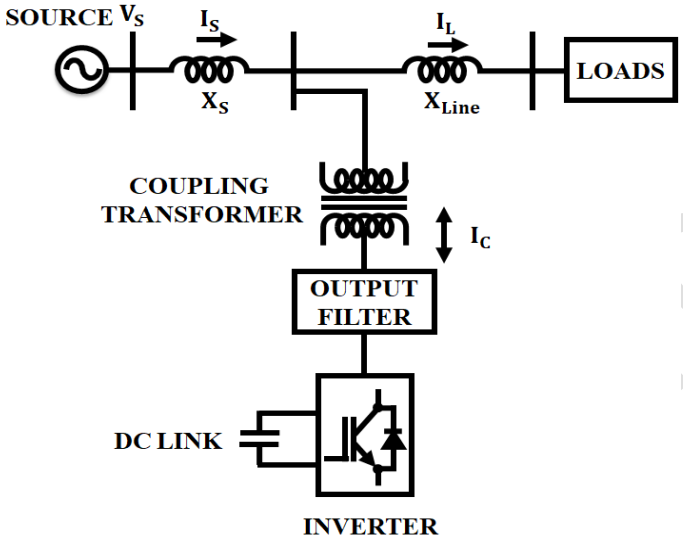

Fig. 3. D-STATCOM structure

In addition to this a coupling transformer is utilized for connecting the voltage level distribution and reactive power magnitude and direction is managed by adjusting output voltage of inverter corresponding to system voltage. As a result of system reactive power is produced, voltage being less than that of VSI AC output voltage. D-STATCOM is representing using in Eq. (1),

$$p\begin{bmatrix} i_a \\ i_b \\ i_c \end{bmatrix} = \begin{bmatrix} -R/L & 0 & 0 \\ 0 & -R/L & 0 \\ 0 & 0 & -R/L \end{bmatrix} \begin{bmatrix} i_a \\ i_b \\ i_c \end{bmatrix} + \frac{1}{L}\begin{bmatrix} e_a - v_a \\ e_b - v_b \\ e_c - v_c \end{bmatrix} \quad (1)$$

As the system is three-phase balance, according to park's transformation in Eq. (2), SRF designing is attained using,

$$p\begin{bmatrix} i_d \\ i_q \end{bmatrix} = \begin{bmatrix} -R/L & \omega \\ \omega & -R/L \end{bmatrix} \begin{bmatrix} i_d \\ i_q \end{bmatrix} + \frac{1}{L}\begin{bmatrix} e_d - v_d \\ e_q - v_q \end{bmatrix} \quad (2)$$

10.22060/EEJ.2026.25286.5894

Where, ω refers to the reference angular speed and v is the PCC voltage and it is calculated always, this transformation makes the d-axis stay at the space vector point voltage connection, where v_q is always kept at zero ($v_q = 0$). Hence, ω implies the space vector angular speed. During steady state conditions, dc and ω is similar to the system frequency. The power introduced into D-STATCOM is determined on the basis of instantaneous real and reactive power which is evaluated in Eq. (3) and (4),

$$p = \frac{3}{2}|v||i|\cos\varnothing = \frac{3}{2}\left(v_d i_d + v_q i_q\right) = \frac{3}{2} v_d\, i_d \left(\therefore v_q = 0\right) \tag{3}$$

$$Q = \frac{3}{2}|v||i|\sin\varnothing = \frac{3}{2}\left(v_d i_q - v_q i_d\right) = \frac{3}{2} v_d\, i_q \left(\therefore v_q = 0\right) \tag{4}$$

Here, p and Q are proportional to i_d and i_q and control power fed into the system is minimized to the control of i_d and i_q. As v_d is consistently measurable, input for the control are fixed arbitrarily and e_d and e_q is maintained by the converter. The varying DC is evaluated using Eq. (5) without considering the inverter losses,

$$\frac{d\left(V_{dc}^2\right)}{dt} = \frac{2}{C} P_e \text{ Where, } P_e = e_d\, i_d + e_q\, i_q \tag{5}$$

Where, P_e denotes the power introduced into AC system by the converter. The current instruction in d-axis and q-axis is attained using regulator in Eq. (6) and (7),

$$i_d^* = \left(k_1 + \frac{k_2}{s}\right).\left(V_{dc}^* - V_{dc}\right) \tag{6}$$

$$i_q^* = \frac{2}{3 v_d} Q^* \tag{7}$$

To further improve D-STATCOM performance and to produce reference current for the DC-Link, DQ/NN-SRF theory is utilized which is detailed below.

2-2- Modelling of DQ Theory/NN-SRF Theory

10.22060/EEJ.2026.25286.5894

The D-Q theory approach enables current extraction by selecting harmonic frequencies and then redeeming it, which in turns increases computational complexity. Hence, more uncomplicated technique is to locate the most essential component of the load current and later utilize it for identifying the other components reasonable for harmonics and reactive power generation. Eq. (8) describes extraction of basic active component of load current.

$$i_{na}(t) = i_1 - i_a(t) \tag{8}$$

Where, $i_a\ (t)$ represents active real power utilized by non-linear load. D-Q theory in Fig.4 is specifically designed for three phase system, where initial transferred orthogonal represents power components. Phase Locked Loop subsystem is utilized for synchronizing the signal for transformation, which is attained using in Eq. (9),

$$\begin{bmatrix} i_{l,a} \\ i_{l,\beta} \end{bmatrix} = \begin{bmatrix} i_l(\omega t) \\ i_l(\omega t - 90) \end{bmatrix} \tag{9}$$

The active and reactive component in d-q frame describe in Eq. (10),

$$\begin{bmatrix} i_d \\ i_q \end{bmatrix} = \begin{bmatrix} \cos\theta & -\cos\theta \\ \cos\theta & \sin\theta \end{bmatrix} \begin{bmatrix} i_\alpha \\ i_\beta \end{bmatrix} \tag{10}$$

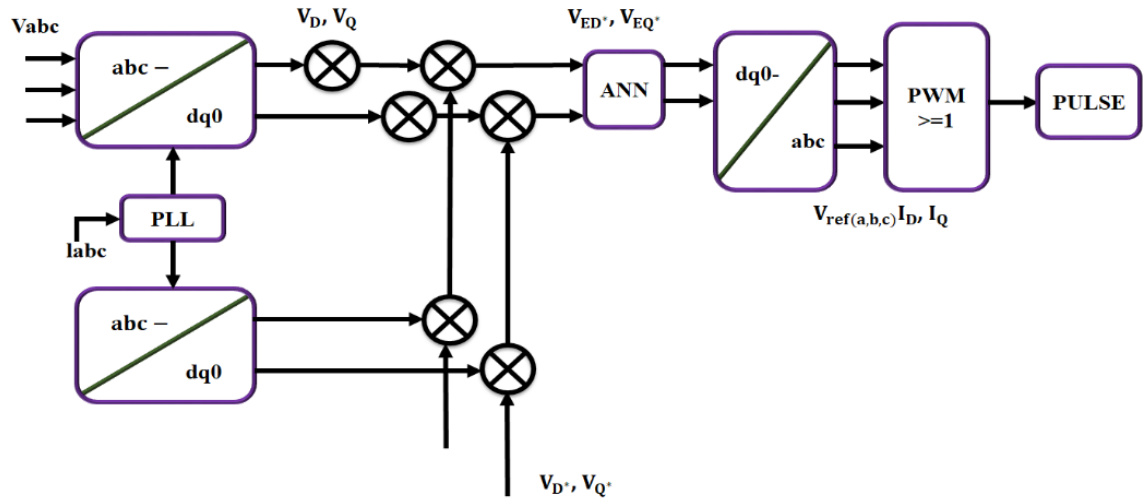

Fig. 4. DQ Theory/NN-SRF Theory

10.22060/EEJ.2026.25286.5894

The essential active and reactive components are DC term's in d-q axis, whereas, harmonic active and reactive component reasonable for distortion power are $i\tilde{L}_d$ and $i\tilde{L}_q$. To distinguish these component on the basis of the requirement's filtering process is performed. The DC components i_d and i_q are extracted using the SRF control and DC components are i_{ddc} and i_{qdc} are converted into reverse park's transformation ($\propto -\beta$) frame. Eq. (11) represents inverse Park's transformation for generation three phase reference current.

$$\begin{bmatrix} i_{\propto dc} \\ i_{\beta dc} \end{bmatrix} = \begin{bmatrix} cos\theta & sin\theta \\ -sin\theta & cos\theta \end{bmatrix} \begin{bmatrix} i_{ddc} \\ i_{qdc} \end{bmatrix} \tag{11}$$

Here, i_{abc} attained is the current transformation, 'Q' compensation is provided as it is zero to evaluate reference source current $i_{ref,abc}$.

Control Approach: To determine $i_{ref,abc}$ by load current component that is absorbed from SRF, switching DSTATCOM is used. The DSTATCOM device additionally needs an AC supply to achieve real power (P) to load and losses. Losses are then calculated using NN control. DSTATCOM with NN controller is developed to enhance its dynamic performance. ANN network as displays in Fig. 5 consists of three layers with each layer containing their own neurons, where input layer comprises of one neuron, hidden layer consists of ten neurons and output layer utilizes single neuron and output obtained is regarded as reference current evaluation. Each layer is deployed with an activation function for training purpose. Using this activation function the input layer which is also the hyperbolic tangent sigmoidal transfer function, while, the output layer activating function is the identity transfer function.

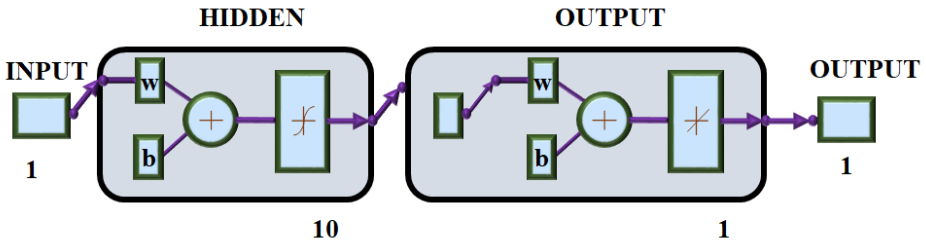

Fig. 5. NN Controller

10.22060/EEJ.2026.25286.5894

Neural Network Architecture and Training

The NN used in the proposed DSTATCOM control has a three-layer feedforward design, involves an input layer, one hidden layer, and an output layer.

Input: DC-link voltage error.

Output: Active current component for loss compensation.

The hidden layer has 10 neurons with a tangent sigmoid activation function, yet output layer has a linear activation function. The network is trained using a supervised learning method with data from offline MATLAB/Simulink simulations of different load and voltage circumstances. The Levenberg-Marquardt backpropagation algorithm is utilized for training.

In addition to this, HCC is also deployed to D-STATCOM architecture for comparing generated reference current with actual load current, thus, enabling to calculate harmonic distortion and reactive power to enhance system constancy and dependability.

2-3- Modelling of Hysteresis Current Controller

The HCC for D-STATCOM as structured in Fig. 6, is developed to minimize switching frequency and current error. The current equation is expressed as,

$$\frac{di_d}{dt} = -\frac{R}{L}.i_d + \omega.i_q + \frac{1}{L}.\left(e_d - v_d\right) \tag{12}$$

$$\frac{di_q}{dt} = -\frac{R}{L}.i_q - \omega.i_d + \frac{1}{L}.e_q \tag{13}$$

Eq. (12) shows the instantaneous current error between reference and real current. Eq. (13) represents the rate of change in current error. Consider, sampling time (T_s) is less, then current equation is represented as,

10.22060/EEJ.2026.25286.5894

$$\frac{di_d}{dt} \rightarrow \frac{i_{d.\ ref}\left(K+1\right)-i_d\left(K\right)}{T_s} \tag{14}$$

$$\frac{di_q}{dt} \rightarrow \frac{i_{q.\ ref}\left(K+1\right)-i_q\left(k\right)}{T_s} \tag{15}$$

Eq. (14) represents the current approximation over a small sample interval. Eq. (15) represents the current deviation inside the hysteresis band. On substituting,

$$\frac{T_s}{L}.\left(e_d\left(K\right)-v_d\right)=\frac{i_{d.\ ref}\left(K+1\right)-i_d\left(K\right)\left(1-\frac{R.T_s}{L}\right)-\omega.T_s.i_q\left(K\right)}{error-_d} \tag{16}$$

$$\frac{T_s}{L}.e_q\left(K\right)=\frac{i_{q.\ ref}\left(K+1\right)-i_q\left(K\right)\left(1-\frac{R.T_s}{L}\right)-\omega.T_s.i_d\left(K\right)}{error-_q} \tag{17}$$

Eq. (16) shows the inverter output voltage as a function of current error. Eq. (17) regulated current tracking within hysteresis limits. Inverter output voltage is proportional to error value obtained, attained error is regarded as the coupling component among the d-axis and the q-axis in SRF reference frame and HCC maintains current error within bands, which is depicted as,

$$lowerband \le i_{d_{ref}} - i_d \le upperband \tag{18}$$

$$lowerband \le i_{q_{ref}} - i_q \le upperband \tag{19}$$

Eq. (18) and (19) is upper and lower hysteresis band condition. The band positions of HCC is altered as, HCC uses the new error term, thus, the new band obtained is introduced using,

$$d-axis:\frac{R.T_s}{L}.i_d-\omega.T_s.i_q \tag{20}$$

$$q-axis:\frac{R.T_s}{L}.i_q+\omega.T_s.i_d \tag{21}$$

10.22060/EEJ.2026.25286.5894

Eq. (20) represents adaptive hysteresis band adjustment. Eq. (21) illustrates stable current regulation with adaptive hysteresis control.

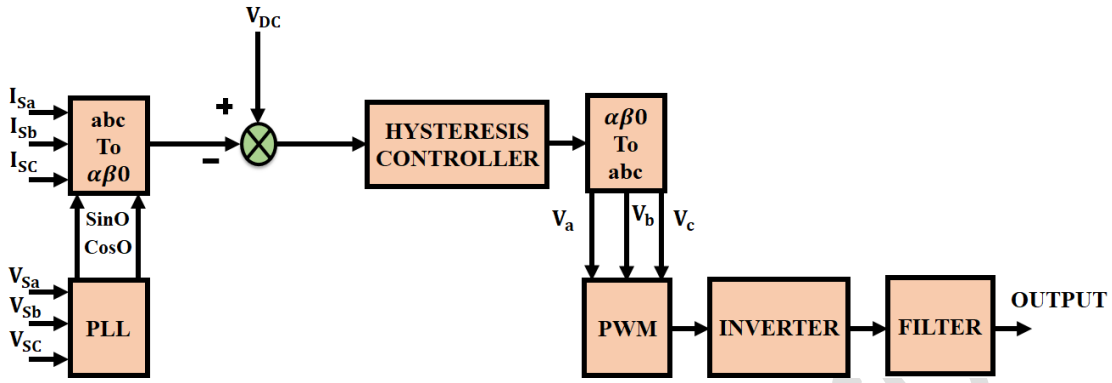

Fig. 6. HCC for D-STATCOM

PI controller and hysteresis band selection

The PI controller gains utilized for DC-link voltage regulation were chosen utilizing a systematic trial-based tuning method. Initially, the proportional gain was increased to provide a quick transient response, while the integral gain was altered to reduce steady-state inaccuracy while avoiding oscillations. The hysteresis band width is determined by balancing current tracking precision and switching frequency. A stronger band enhances current tracking but increases switching losses, whereas a larger band decreases switching frequency while increasing current ripple. Based on this trade-off, the hysteresis band was chosen to provide steady current regulation with an appropriate switching frequency and low ripple.

Significantly, to provide sufficient to meet the power necessities of DC-link, PV system is utilized which provides clean and unlimited energy supply.

2-4- Modelling of PV system

A solar cell generally consists of p-n semiconductor junction which when exposed to sunlight produces current. The produced current normally depends on solar irradiance and temperature level. Fig. 7 illustrates equivalent diagram of PV system, and it is mathematically represented in Eq. (22),

10.22060/EEJ.2026.25286.5894

$$I = I_{ph} - I_0 \tag{22}$$

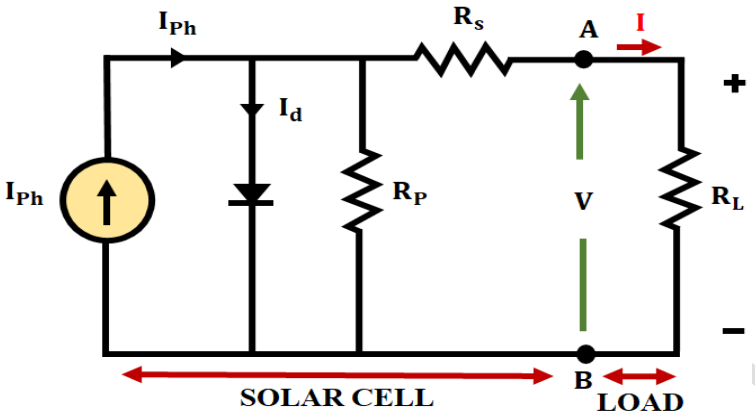

Fig. 7. PV system

The (I-V) features equation of PV system is expressed in Eq. (23),

$$I = I_L - I_0\left(e^{\frac{q(V+IR_s)}{kT}} - 1\right) - \frac{V+IR_s}{IR_p} \tag{23}$$

Where, I_L represents the sunlight generated current, I_0 refers to the diode current, R_s and R_P implies the series and shunt resistance current, T stands temperature, K stands Boltzmann constant, q represents charge of electron and V indicates the output voltage respectively. However, the initial output produced by PV is quite low, hence, Re-Lift SEPIC converter is integrated into the PV system.

2-5- Modelling of Re-Lift SEPIC Converter

Re-lift SEPIC converter is deployed for boosting PV power output which is depicted in Fig. 8. Re-lift SEPIC converter comprises of two switches S_1 and S_2, four diodes D_1, D_2, D_3 and D_4, four capacitors C_0, C_1, C_2 and C_3 and lastly two inductor L_1 and L_2 respectively.

10.22060/EEJ.2026.25286.5894

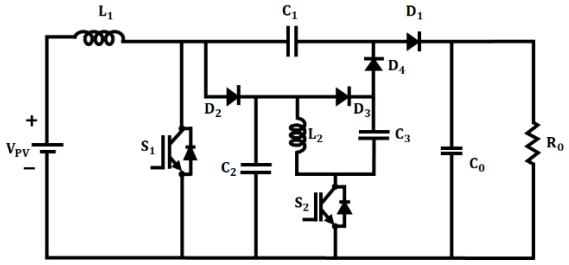

Fig. 8. Re-Lift SEPIC converter

The Re-lift SEPIC converter functions in two modes namely, mode 1 and mode 2, which are exposed in Fig. 9. Eqs. (24)-25 represent the inductor voltage and capacitor charging equations in Mode-1 operation, when both switches are turned on and energy is stored in the converter components.

$$V_{C_2} + V_{L_2} - V_{C_3} - V_0 = 0 \tag{24}$$

$$V_{L_2} - V_{C_3} + V_{C_1} = 0 \tag{25}$$

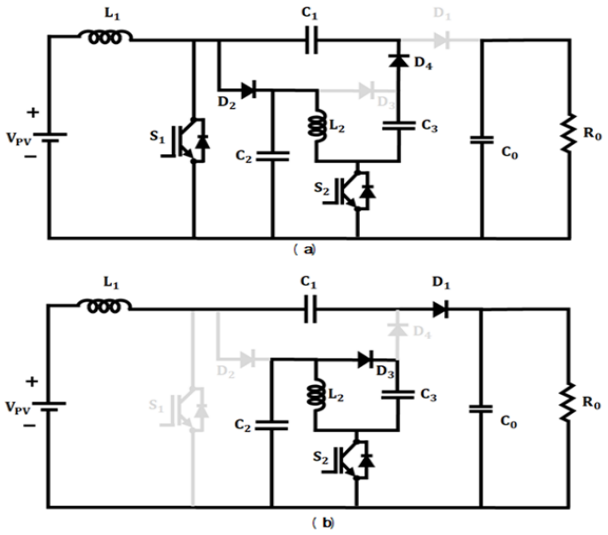

Fig. 9. Modes of Operation

Mode 1: S_1 and S_2 are kept in ON state, along with diode D_2 and D_4 respectively. Whereas, capacitor C_2 and C_3 gets charged along with inductor L_1. Therefore, C_1 and C_0 gets discharged, while C_0 discharges and supplies to the load.

10.22060/EEJ.2026.25286.5894

$$V_{PV} = V_{L_1} \tag{26}$$

$$V_{PV} = V_{C_2} \tag{27}$$

$$V_{C_2} + V_{L_2} = 0 \tag{28}$$

$$V_{L_2} - V_{C_3} + V_{C_1} = 0 \tag{29}$$

$$V_{C_0} = V_0 \tag{30}$$

Eqs. (26)-30 describe the current fluctuation, energy transfer, voltage stress, and capacitor voltage balance relationships during Mode-1, as well as the power flow from the PV source to the load.

Mode 2: In this mode, Switch S_1 turned OFF, while S_2 is kept in ON state, together with diode D_3 and D_1 respectively. Whereas, capacitor C_2 and inductor L_2 are discharging and the power flows through the diode.

$$V_{PV} - V_{L_1} - V_{C_1} - V_{C_0} = 0 \tag{31}$$

$$V_{C_0} = V_0 \tag{32}$$

Eqs. (31)-(32) are the inductor voltage and capacitor discharge equations for Mode-2 operation, which occurs when one switch is turned off and stored energy is supplied to the output.

On substituting,

$$V_{PV} - V_{L_1} - V_{C_1} - V_0 = 0 \tag{33}$$

$$V_{C_2} = V_{L_2} \tag{34}$$

$$V_{L_2} = -V_{C_3} \tag{35}$$

10.22060/EEJ.2026.25286.5894

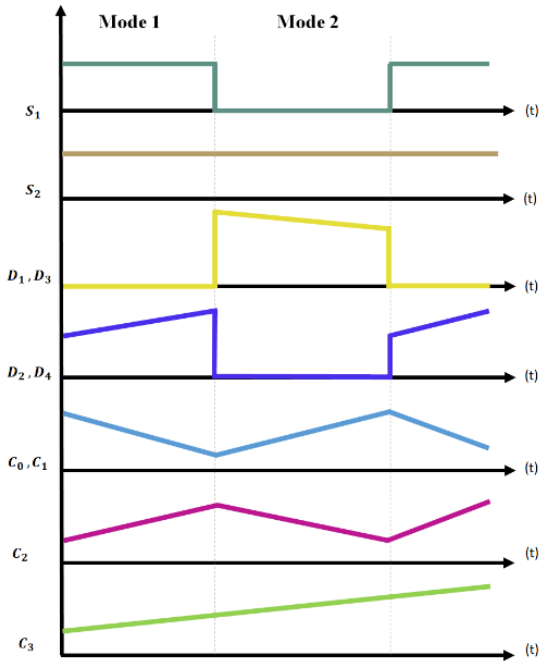

Fig. 10. Timing Diagram

Eqs. (33)-(35) show the output voltage, voltage gain, and steady-state operating conditions of the Re-Lift SEPIC converter. Fig. 10 represents the timing waveform of Re-Lift SEPIC converter. Therefore, the proposed system ensures to attain improved PQ using DSTATCOM with DQ/NN-SRF theory.

State space modelling and dynamic analysis of Re-Lift SEPIC converter

A state-space model is constructed to examine the Re-Lift SEPIC converter's dynamic behavior and to aid in controller design. The converter dynamics are characterized using inductor currents and capacitor voltages as state variables. The state vector of the converter defines as,

$$x = \left[i_{L1}, i_{L2}, v_{C1}, v_{C2} \right]^T \tag{36}$$

Here, i_{L1} and i_{L2} stands inductor currents and v_{C1} and v_{C2} stands capacitor voltage.

Mode 1 (Switched ON)

During this mode, energy is kept in the inductor and capacitors. The state equations are given by,

$$i_{L1} = \frac{V_{pv}}{L_1},\ i_{L2} = \frac{v_{C1}}{L_2} \tag{37}$$

$$v_{C1} = \frac{i_{L2}}{C_1},\ v_{C2} = -\frac{i_0}{C_2} \tag{38}$$

Mode 2 (Switched OFF):

In this mode, stored energy is transferred to the load. Thee corresponding state equations are expressed as.

$$i_{L1} = \frac{V_{pv} - v_{C2}}{L_1},\ \ i_{L2} = \frac{v_0}{L_2} \tag{39}$$

$$v_{C1} = -\frac{i_{L2}}{C_1},\ v_{C2} = \frac{i_{L1}}{C_2} \tag{40}$$

The resulting state-space model confirms the Re-Lift SEPIC converter's steady performance in continuous conduction mode and serves as a foundation for dynamic analysis and PI controller design in the DC-link voltage regulation system.

4. Results And Discussion

This section discusses and elaborates on the suggested system utilizing MATLAB/Simulink implementation, the results achieved, and a comparative analysis of them.. Table 2 showcases parameter specifications of developed system.

Table 2. Parameter Specification

Parameters	Values
PV System	
Open circuit voltage	37.25V
Number of cells connected in parallel	2
Short circuit current	8.95A
Number of cells connected in series	17
Re-Lift SEPIC Converter	
C_1, C_2, C_3	$22\mu F$
L_1, L_2	$4.7mH$
Switching Frequency	$10KHz$
C_0	$2200\mu F$

Case 1: Varying Temperature and Intensity

10.22060/EEJ.2026.25286.5894

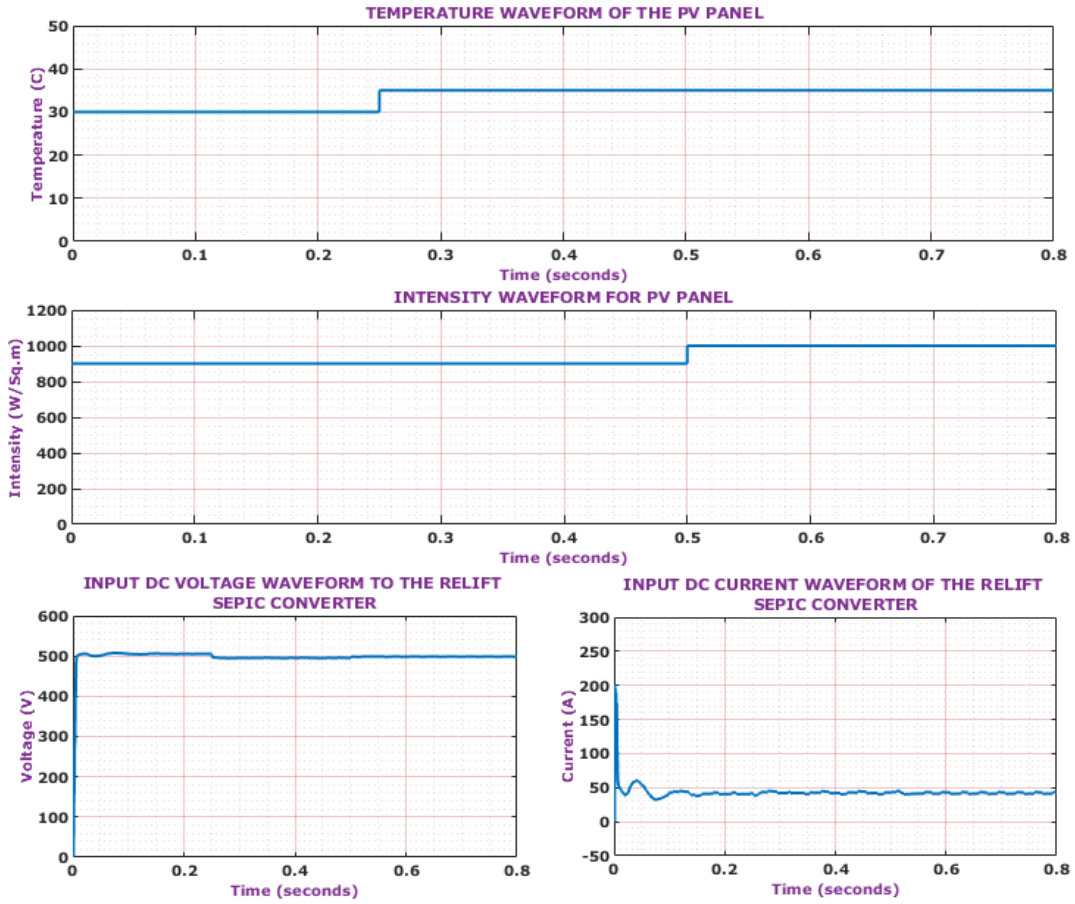

Fig. 11. PV panel behaviour/ Input DC voltage and current waveform

Fig. 11 represents the PV panel and Re-Lift SEPIC converter performance waveform under varying temperature and intensity. The PV panel temperature and intensity, where both the temperature and intensity initially begins with steady temperature of 30°C and intensity of 900 W/Sq-m, where after 0.2 seconds the panel temperature increases to 35°C and at 0.5 seconds the PV Panel intensity lightly growths to 1000 W/Sq-m. Significantly, the input DC current and voltage waveform, where both voltage and current undergoes certain fluctuations throughout the given time duration of 0.8 seconds respectively.

10.22060/EEJ.2026.25286.5894

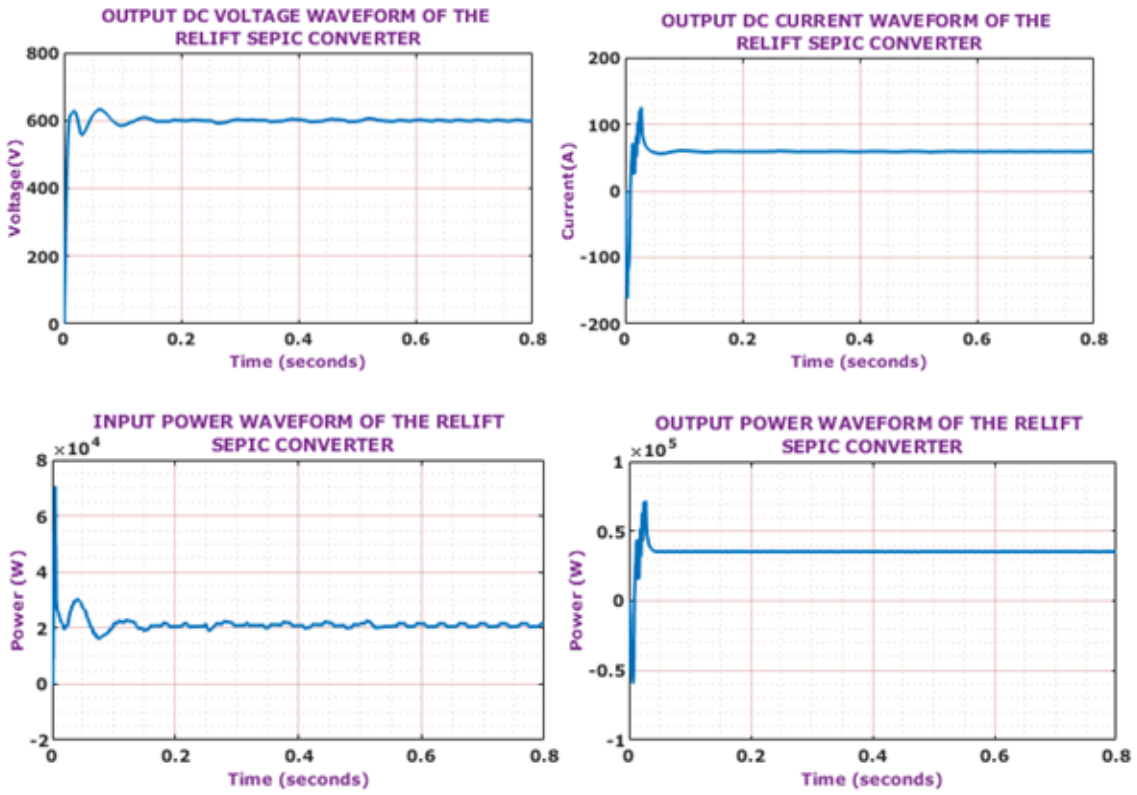

Fig. 12. Re-Lift SEPIC converter performance waveform

Fig. 12 shows output voltage/current and input/output power of Re-Lift SEPIC converter. Initially, output voltage starts with rapid rise and deviates before settling down at 600 V, similarly, the output current also rapidly increases before settling down at 60 A respectively. Consecutively, the third and fourth graph shows that, input power is maintained at 2×10^4 W throughout 0.8 seconds and oscillations in the line depicts the fluctuations within the input power and the output power, rapidly increases beyond 0.5×10^5 W and further drops down to 0.4×10^5 W and maintained with zero fluctuations.

10.22060/EEJ.2026.25286.5894

Case 2: Constant Temperature and Intensity

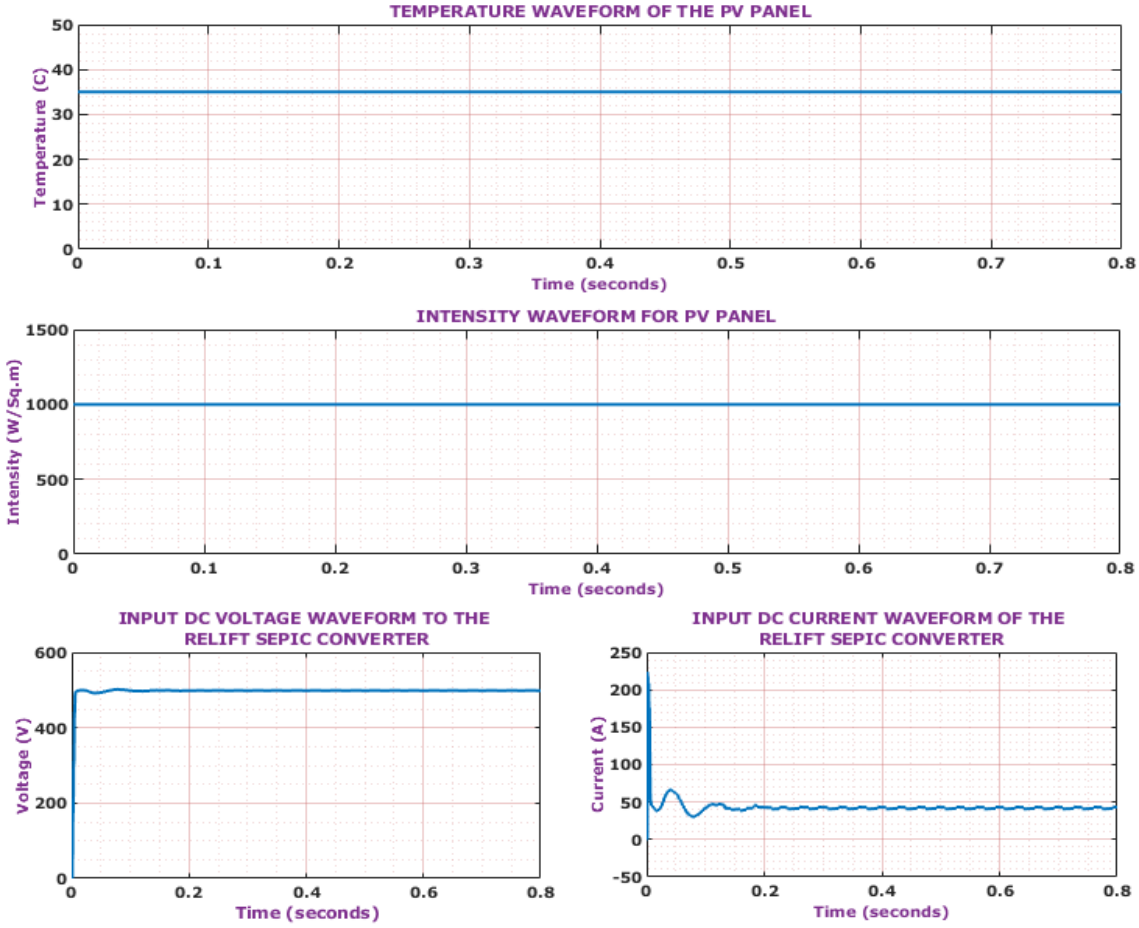

Fig. 13. PV panel and Input DC voltage/current of Re-Lift SEPIC converter

The first and second plot in Fig. 13 showcases PV panel performance waveform under constant conditions. Both temperature and intensity are maintained at of 35°C and 1000 W/Sq-m with smooth line, indicating the absence of deviations. Significantly, the third and fourth graph showcases that, input DC voltage rapidly rises beyond 400V before settling down at 550V and DC current primarily decrease and then continued at 55 A throughout the showed time period of 0.8 seconds respectively.

10.22060/EEJ.2026.25286.5894

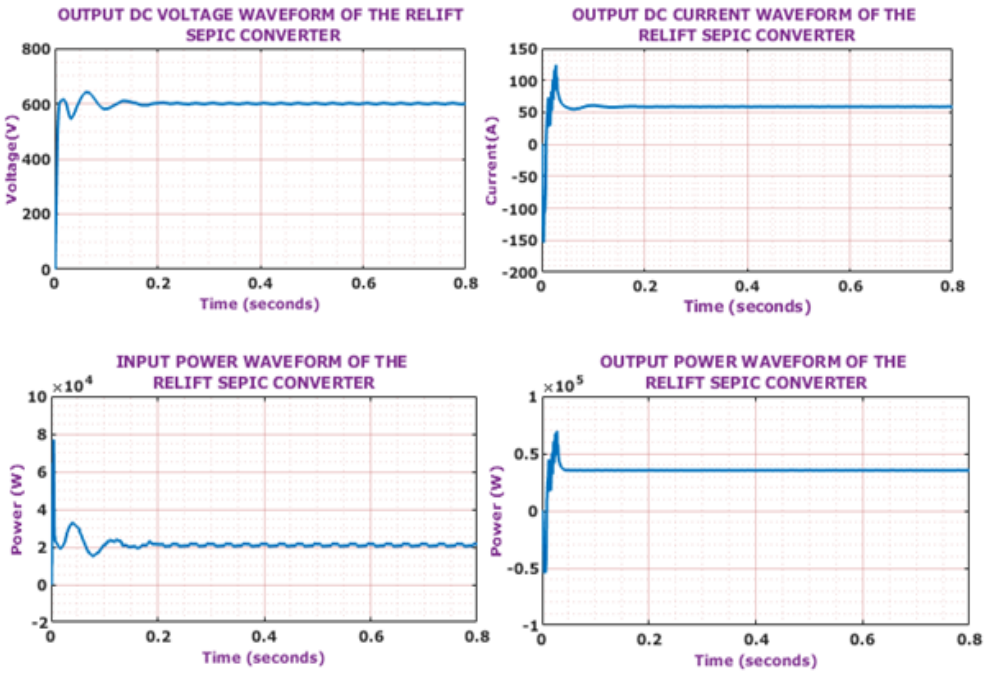

Fig. 14. Output voltage/current and input/output power waveform

Fig. 14 denotes the output voltage and current waveform, both voltage and current rises rapidly before voltage stabilizing at 600 V and current stabilizing at 51 A respectively. Consecutively, Input power initially drops down to 2×10^4 W and further stabilized, the output power rapidly rises beyond 0.5×10^5 W and later stabilizes at 0.3×10^5 W, indicating the efficient power supply to meet the system power requirements.

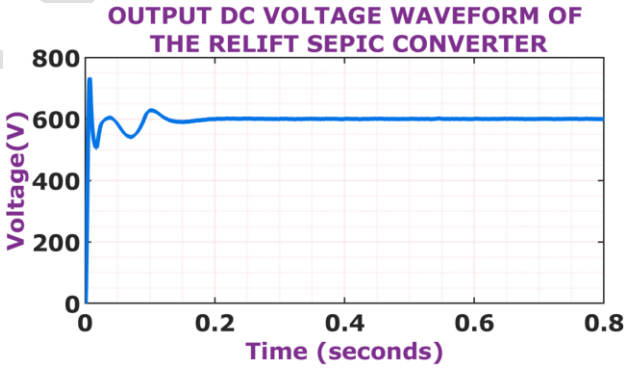

Fig.15 Output DC Voltage Waveform of Re-Lift SEPIC Converter.

Fig. 15 depicts output DC voltage response of the Re-Lift SEPIC converter. Due to initial dynamics, there is a small transient overshoot, yet the voltage quickly settles and remains stable at around 600 V, showing excellent voltage regulation and converter steady-state stability.

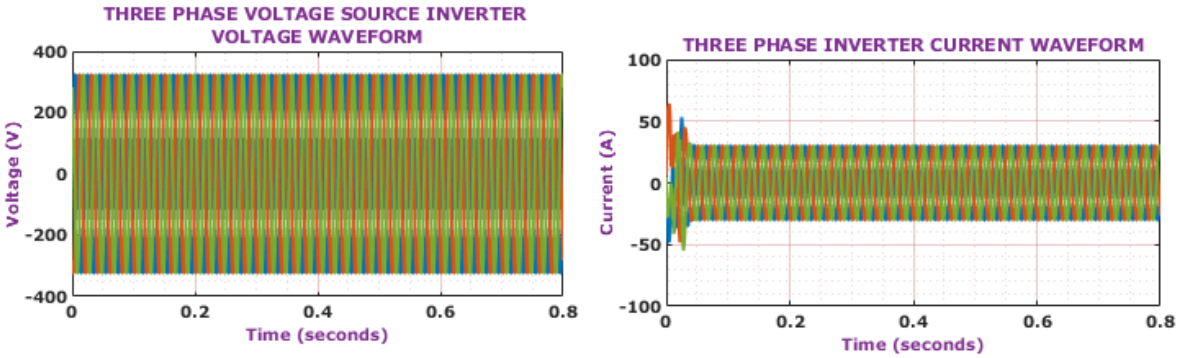

Fig. 16. Three Phase VSI voltage/current

Fig. 16 refers to the waveform comprising of three phase VSI voltage and current, where the voltage is continued between ±300 V throughout at 0.8 s and current at first starts with slight fluctuations prior to stabilizing between ±30 A respectively, implying consistent and sustainable system performance under varying load conditions.

4-1- Zoom view of grid inverter voltage and current waveform

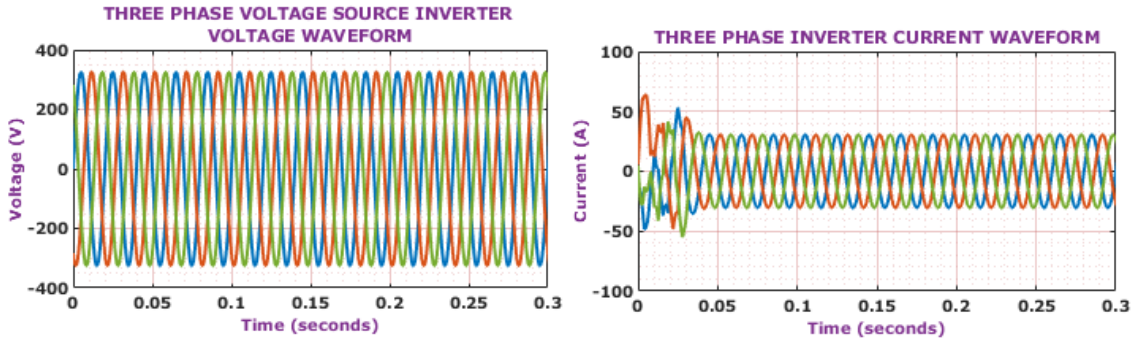

Fig. 17. Three Phase VSI voltage/current in zoom view

10.22060/EEJ.2026.25286.5894

Fig. 17 displays three phase VSI voltage and current waveform, where voltage is constantly sustained between ± 300 V at 0.3 s. Considerably, three phase VSI current initially begins with certain fluctuations preceding to settle down between ±30 A respectively.

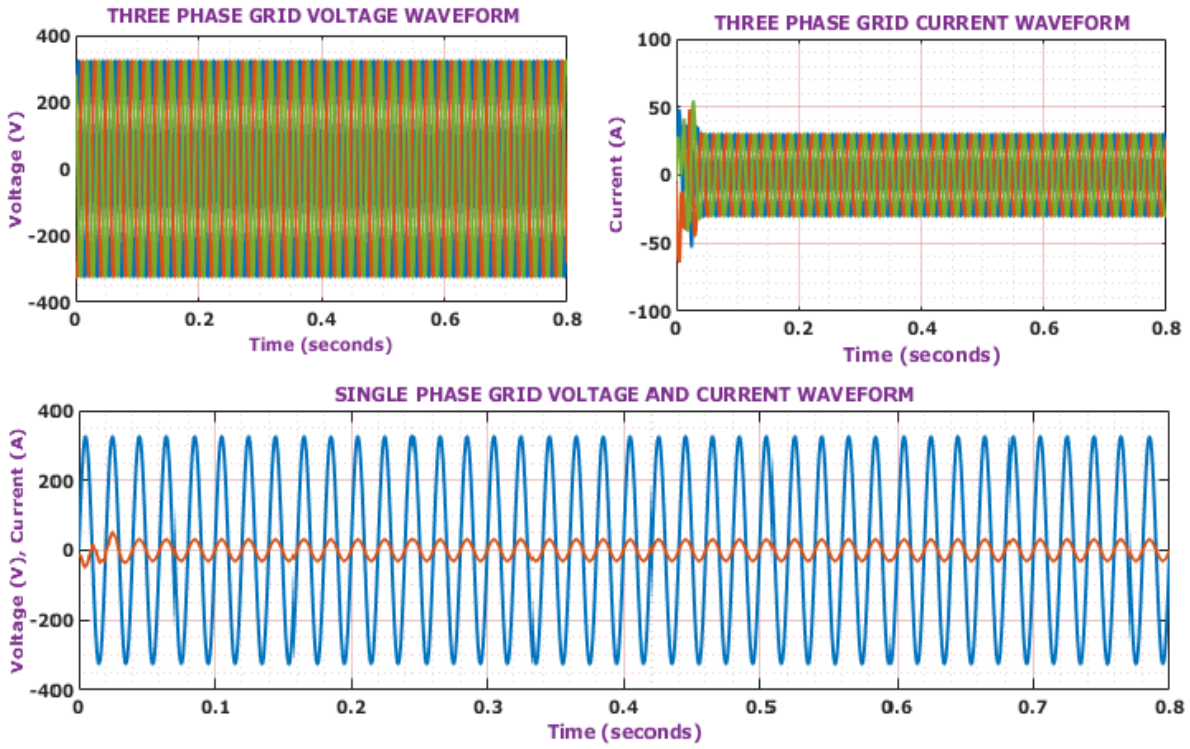

Fig. 18. Three Phase Grid performance matrices

Fig. 18 demonstrates three phase grid and single-phase grid waveforms, where grid voltage is continued between ± 300 V from very beginning, indicating smooth and non-fluctuated voltage. Furthermore, the three phase grid current begins with slight deviations before stabilizing at the range of ±30 A respectively. And lastly, the third graph showcases the single-phase grid existing in perfect synchronization, indicating stable and consistent functioning.

10.22060/EEJ.2026.25286.5894

4-2- Zoom view of grid voltage and current waveform

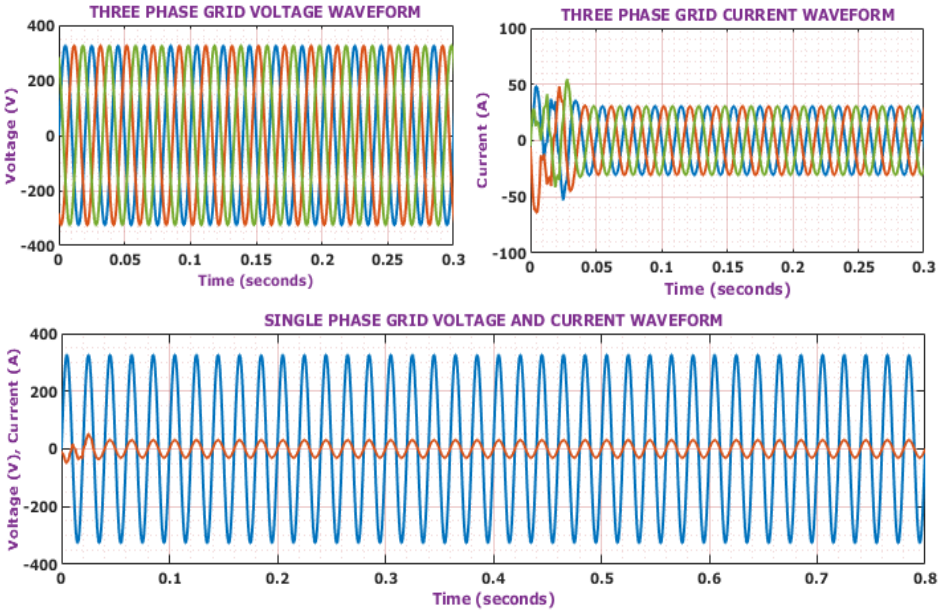

Fig. 19. Zoom view of three phase grid voltage and current

Fig. 19 represents three phase grid voltage/current and single-phase voltage/current in zoom view, where voltage of three phase grid is maintained between ±300 V from the beginning till the end of the given time duration. The second graph shows the three-phase grid current waveform, where current initially begins with minor fluctuations before settling down at the range of ±30 A respectively. And the third waveform of single-phase grid, which showcases perfect synchronization of voltage and current, implying balanced power transmission.

10.22060/EEJ.2026.25286.5894

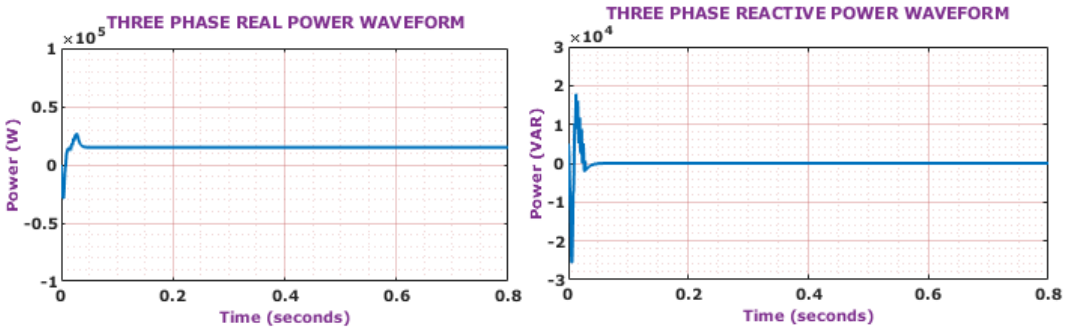

Fig. 20. Real and Reactive Power Waveform

Fig. 20 showcases real and reactive power waveform, in which both real and reactive power faces certain deviations at the beginning prior to stabilizing. The real power stabilizes at 0.2×10^5 and the reactive power is maintained at zero, referring to reduced power losses with improved utilization of real power.

4-3- Grid Case 1: 12 Kw

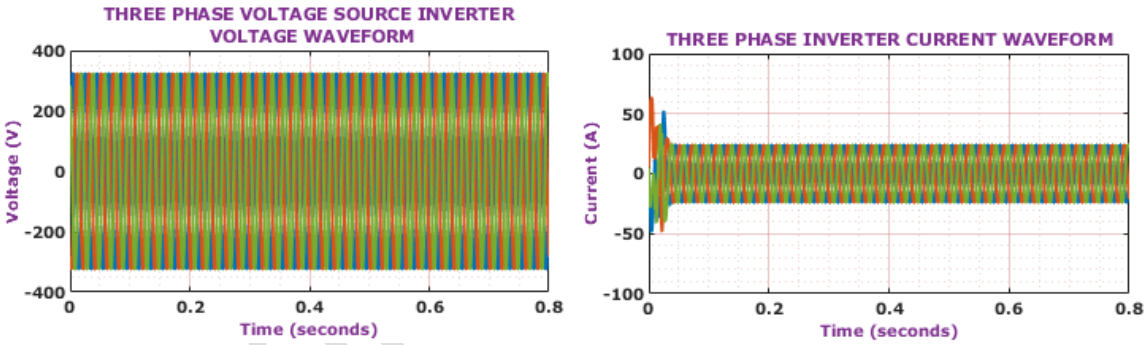

Fig. 21. Three Phase voltage and current waveform of three phase VSI

Fig. 21 displays three phase VSI waveform, where voltage is maintained between ±300 V from the beginning with no fluctuations, implying stable and consistent power supply. Significantly, the three phase inverter current initially undergoes certain fluctuations and later stabilizes between ±20 A respectively.

4-4- Zoom view of grid inverter

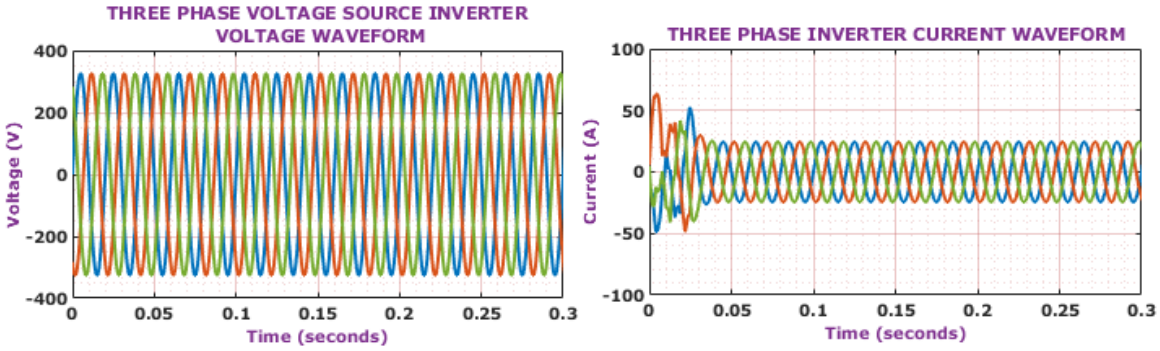

Fig. 22. VSI voltage and current waveform in zoom view

Fig. 22 implies the zoom view of three phase VSI voltage and current waveform, where voltage from the beginning is kept stable between ±300 V, while, current initially goes through certain fluctuations preceding to settle down between ±20 A respectively.

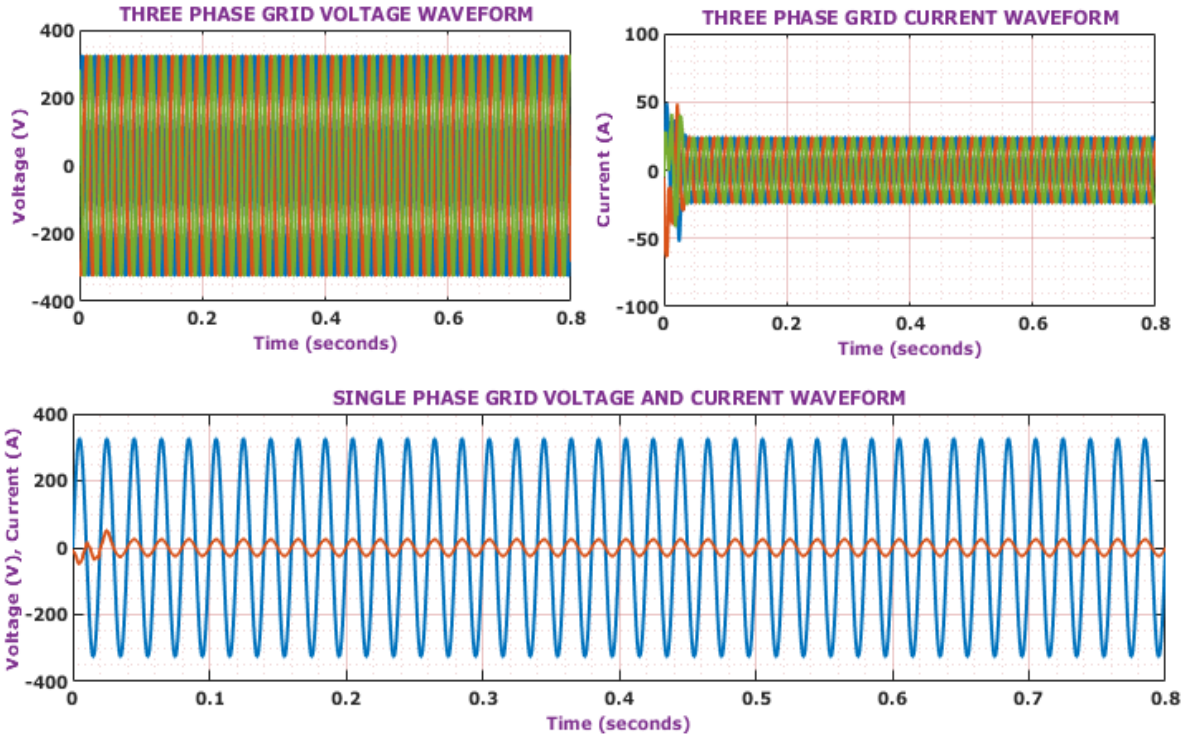

Fig. 23. Three Phase grid and Single-Phase grid waveform

10.22060/EEJ.2026.25286.5894

Fig. 23 represents three phase grid voltage and current along with single phase grid voltage and current waveforms. First graph showcases three phase grid voltage which is maintained between ±300 V and three phase grid current waveform show that, the gird current starts with minor deviations and further stabilizes between ±20 A respectively. Lastly, the third graph displays single-phase grid, where both voltage and current are properly maintained at period of 0.8 s correspondingly.

4-5- Zoom view of grid voltage and current waveform

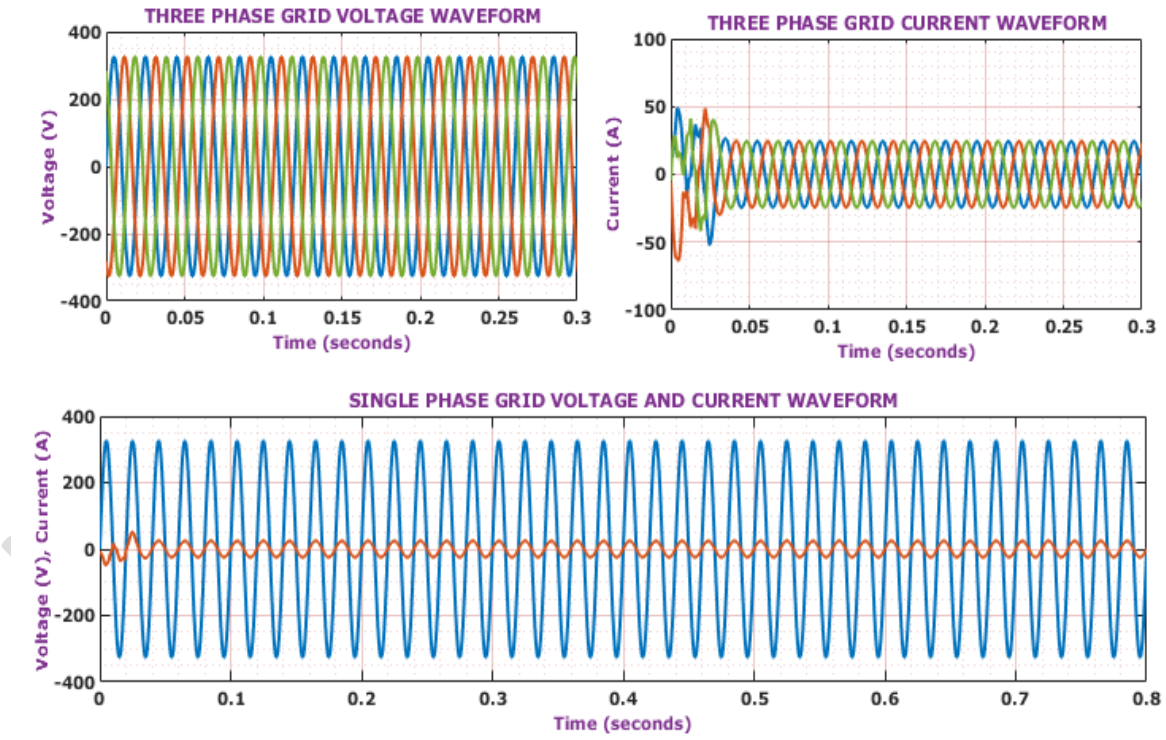

Fig. 24. Zoom view of three phase and single-phase grid waveform

10.22060/EEJ.2026.25286.5894

Fig. 24 showcases three phase grid voltage/current and single-phase grid voltage/current waveform, where grid voltage and current in which grid voltage is stabilized and maintained at the range ±300 V and the second graph show that, current with initial fluctuations is stabilized 0.04 seconds and continued at that specific current. Eventually, third graph shows both the voltage and current waveform of single-phase grid, displaying properly maintained voltage and current throughout entire time duration of 0.8 seconds respectively.

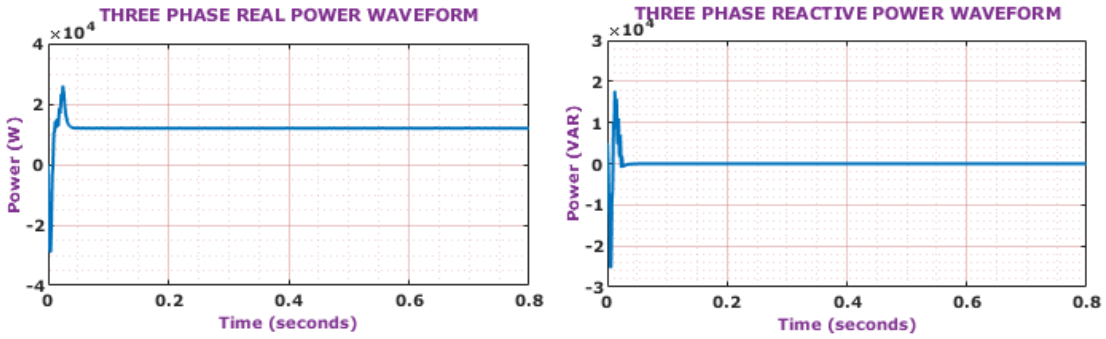

Fig. 25. Three Phase real and reactive power

Fig. 25 represents real and reactive power, initially rapidly rises beyond 2×10^4 W and 1×10^4 VAR before settling down and maintained, indicating minimized power losses with improved real power utilization.

Case 3: Grid Variations (9000-13000)

10.22060/EEJ.2026.25286.5894

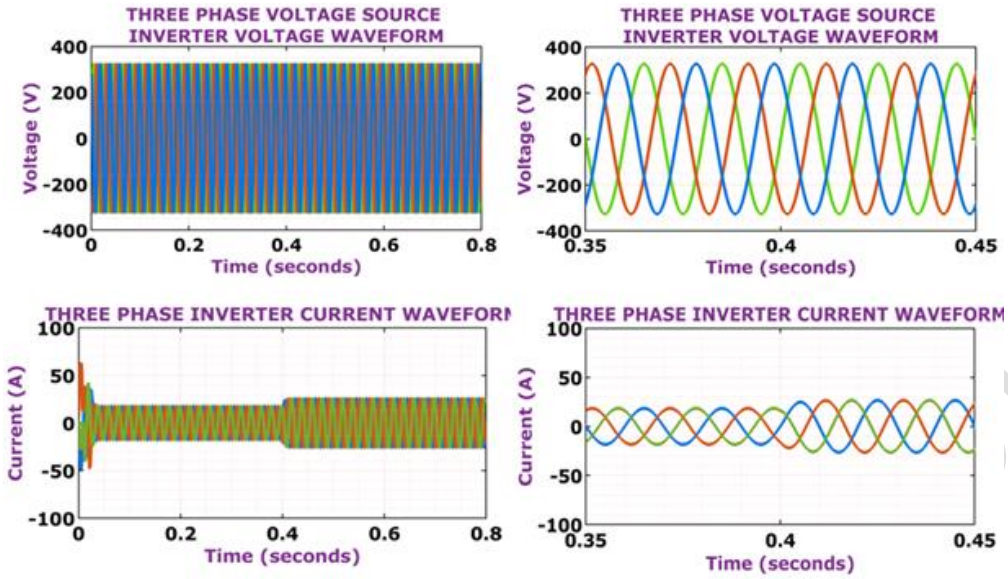

Fig 26. depicts three-phase VSI voltage and current waveforms during grid load variations (9-13 kW).

Fig. 26 displays the three-phase VSI voltage and current waveforms as grid load varies from 9 kW to 13 kW. The inverter voltage is continued at around ±300 V, while current changes from ±20 A to ±30 A based on load change, indicating effective current management and steady operation**.**

10.22060/EEJ.2026.25286.5894

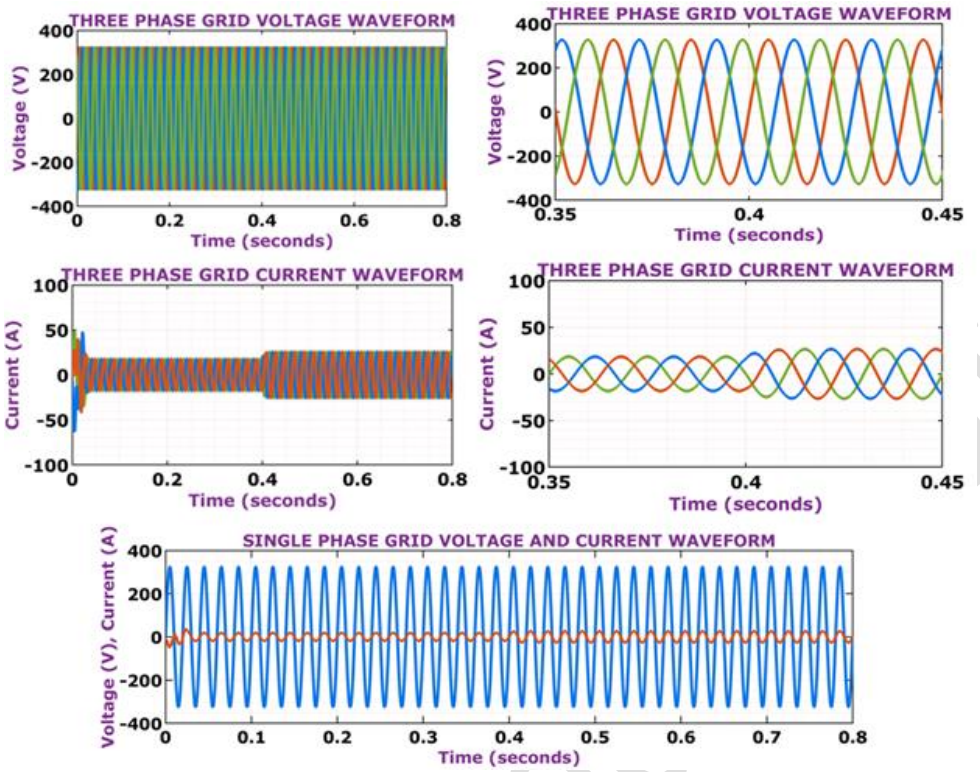

Fig.27. Three-phase grid voltage and current waveforms during load variations (9-13 kW).

Fig. 27 depicts three-phase grid voltage and current at the PCC for load fluctuations ranging from 9 kW to 13 kW. The grid voltage stays regulated at around ±300 V, while the grid current rises from ±20 A to ±30 A, indicating improved PQ and controlled current injection under different grid situations. Single-phase grid waveforms with load ranging from 9 kW to 13 kW. The voltage remains at ±300 V and the current fluctuate appropriately with the load, demonstrating near-unity power factor operating.

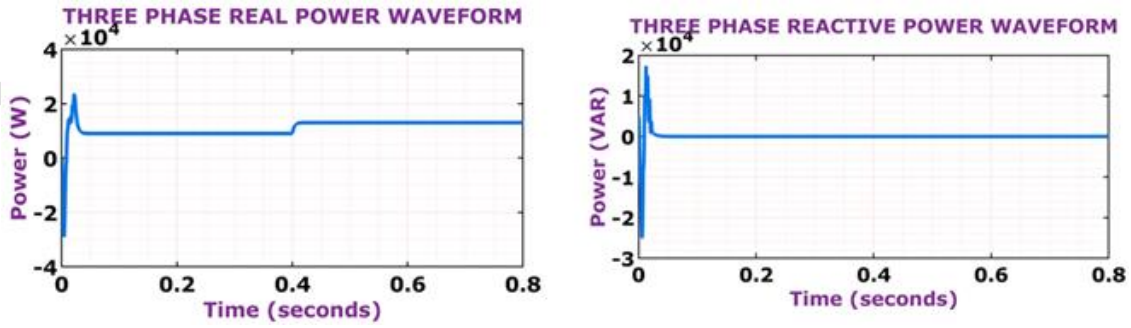

Fig. 28. Three-phase real and reactive power waveforms under grid load variations (9-13 kW).

10.22060/EEJ.2026.25286.5894

Fig.28 displays the system's actual and reactive power responses to grid load fluctuations ranging from 9 to 13 kW. The real power rises from around 9 kW to 13 kW, while the reactive power is efficiently managed close to 1 VAR, proving efficient reactive power compensation and steady system operation.

Closed-Loop Stability Discussion:

The proposed control system's closed-loop stability is ensured by its hierarchical structure, which includes an outside PI-based DC-link voltage control loop and an interior HCC loop. PI controller manages the DC-link voltage with zero steady-state error, but the hysteresis current controller ensures limited current tracking by keeping the current error within predefined bounds, resulting in fast dynamic reaction to load disturbances. The NN-based SRF control serves as an adaptive estimator for reference current generation and loss compensation while avoiding unstable feedback routes. As a result, the total system stays stable under load fluctuations and parameter uncertainties, as seen by the simulation results, which show limited currents, quick settling, and the absence of oscillations.

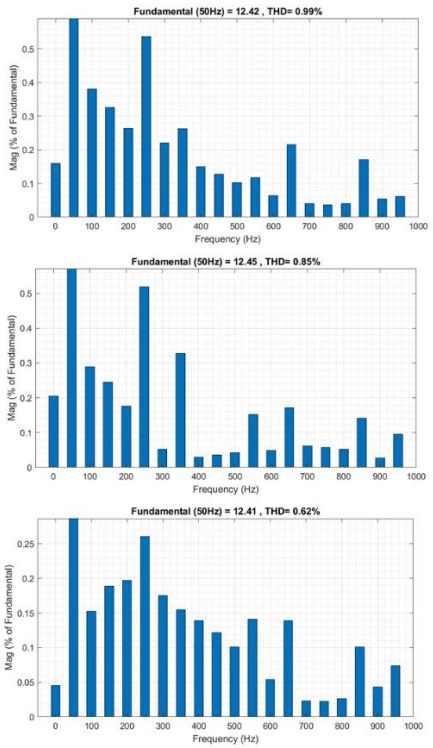

10.22060/EEJ.2026.25286.5894

Fig. 29. THD Waveform

Fig. 29 indicates the THD waveform for Y, R and B phases, where x-axis states frequency in Hz ranging between 0 to 1000 Hz and y-axis represents magnitude. Among all the three plot, the last plot for B phase attained reduced THD value of 0.62%, indicating the reducing THD with improved stability and reliability. The reported THD value of 0.62% corresponds to the source current measured at the PCC during steady-state operation. The THD is calculated using FFT analysis over a single fundamental cycle in line with IEEE 519 PQ requirements. This low THD result indicates the efficiency of the proposed DQ-NN-SRF controlled DSTATCOM in suppressing current harmonics.

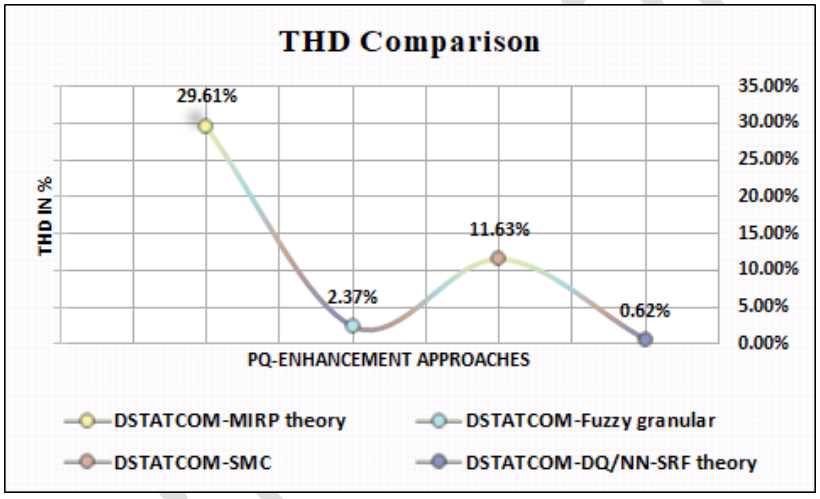

Fig.30. THD Comparison

Fig. 30 showcases the THD comparison chart comprising PQ enhancement approaches various conventional control techniques like DSTATCOM with MIRP theory [20], Fuzzy Granular control [21], SMC [22] and proposed topology using DQ/NN-SRF theory. Proposed approach attained low THD value of 0.62% than that of the other control techniques, indicating improved PQ enhancement performance with reduced harmonics.

10.22060/EEJ.2026.25286.5894

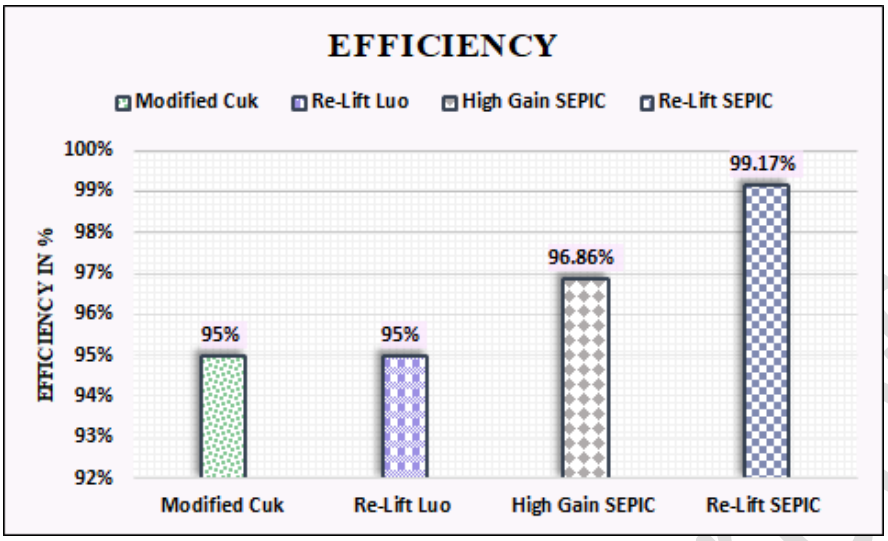

Fig. 31. Comparison of Efficiency

Fig. 31 represents efficiency comparison analysed for various traditional converter with the proposed Re-Lift SEPIC converter to determine its performance capabilities. Here, proposed converter attained quite higher efficiency of 99.17 % than the other converters such as Modified Cuk [23], Re-Lift Luo [24] and High Gain SEPIC [25] which acquired 95%, 95% and 96.86 % respectively, thus implying the improved PV production boosting ability.

The Re-Lift SEPIC converter has an efficiency of 99.17% under rated operating conditions of nominal input voltage and full load. The efficiency estimate includes into consideration the conduction losses of switches and diodes, as well as the copper losses of inductors. Switching and core losses are minimal due to the adoption of high-efficiency components and robust steady-state operation. The converter's efficiency performance is assessed under a variety of load circumstances, including partial and rated load operation. The results show that the converter maintains excellent efficiency throughout the working range, with peak efficiency occurring around the rated load. Under light-load conditions, the increased influence of fixed losses causes a slight drop in efficiency, which is comparable with the behavior of high-gain DC-DC converters.

10.22060/EEJ.2026.25286.5894

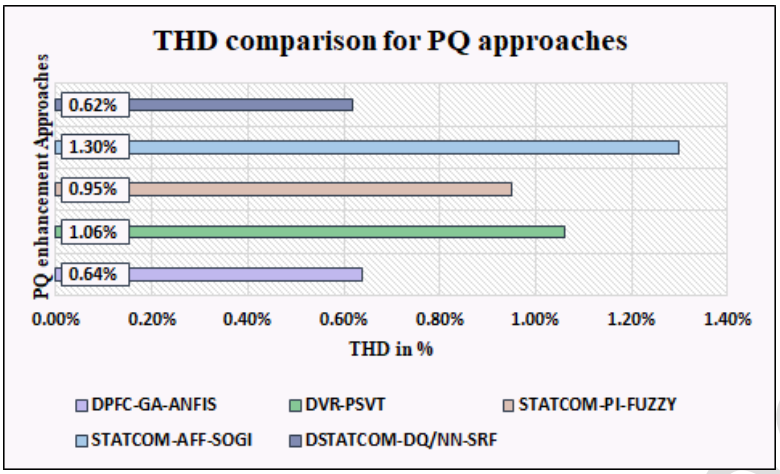

Fig. 32. THD comparison for various PQ enhancement approaches

Fig. 32 refers to the THD comparison chart consisting of different PQ enhancement approaches with their corresponding control techniques along with proposed PQ mitigation approach with its control technique such as DPFC-GA-ANFIS [13], DVR-PSVT [4], STATCOM-PI-Fuzzy [8] and STATCOM-AFF-SOGI [26]. Proposed model attained considerably reduced THD other depicted approaches, indicating developed system performs advanced PQ rectification process with better performance in terms of increased PQ with minimized harmonics.

Table. 3 Quantitative PQ improvement achieved using Propose system

PQ Parameter	Without Compensation	With Proposed Method	Improvement
Voltage THD (%)	6.84	0.62	90.94% reduction
Current THD (%)	7.12	0.62	91.29% reduction
Reactive Power (VAR)	High and fluctuating	Minimal	Near unity compensation
Power Factor	0.82	0.99	Improve to unity
Voltage Regulation	±12%	±1%	Significant stabilization
Harmonic Distortion	Severe	Minimal	IEEE-519 compliant

Table 3 quantitatively illustrates the PQ improvements realized with the proposed DSTATCOM and DQ/NN-SRF management. Significant decreases in voltage and current THD have been noted, reaching 0.62%, which meets IEEE-519 requirements. Reactive power is successfully adjusted, resulting in a near-unity power factor and better voltage regulation at the PCC.

Table 4. Comparison of proposed method with existing DSTATCOM-nase PQ enhancement techniques.

Reference	Control techniques	Renewable Integration	Key Limitation
Fuzzy Granular Control [21]	Fuzzy Logic	No	Slow convergence
SMS based DSTATCOM [22]	Sliding Mode	No	Chattering effect
AFF-SOGI-STATCOM [26]	Adaptive Filter	No	Complex implementation
PROPOSED	DQ/NN-SRF	PV + Re-Lift Sepic	Low complexity, fast response

Unlike previous NN-based DSTATCOM controllers, the proposed strategy combines a DQ/NN-SRF control strategy with a PV-fed Re-Lift SEPIC converter, resulting in greater harmonic mitigation and long-term DC-link regulation. The achieved THD of 0.62% is the lowest among contemporary approaches, indicating higher accuracy, faster dynamic responsiveness, and less computational overhead as shown in Table 4.

5. Conclusion

The proposed system is developed to overcome the PQ issues within distribution system and to rectify them. The integration of DSTATCOM with advanced control approaches ensures better PQ issues mitigation. The utilization of DSTATCOM attained improved PQ, Voltage regulation with dynamic load compensation and reduced harmonic, thus, producing less transmission losses. Significantly, the usage of D-Q theory and N N-SRF theory enables accurate compensation of reactive power and harmonic currents, thereby, improving the overall stability and reliability with minimized distortions at the PCC. Additionally, the incorporation of PV system with Re-lift SEPIC converter produced highly regulated output voltage to meet the power requirements of the developed scheme. To further evaluate efficacy of developed system, MATLAB/Simulink implementation outcomes depicts that, the developed system attained enhanced system performance efficiency with highly improved PQ under varying load conditions. Therefore, the developed system using DSTATCOM assures better PQ mitigation with overall enhanced distribution

system performance. Future study will include hardware implementation and experimental validation to determine the resilience of the suggested control approach in real-world non-ideal conditions.

References

[1] A. Ram, P. R. Sharma, and R. K. Ahuja, "Enhancement of power quality using U-SOGI based control algorithm for DSTATCOM," Ain Shams Engineering Journal, vol. 15, no. 1, pp. 102296, 2019

[2] V. Kushawaha, R. Yadav, A. Rawat, and A. Verma. "Enhancement of voltage profile in transmission line using DSTATCOM and DVR," International Journal of Advanced Computer Technology, vol. 10, no. 6, pp. 01-05, 2021.

[3] P. Kumar, S. R. Arya, K. D. Mistry, and S. Yadav. "A self-tuning ANFIS DC link and ANN-LM controller based DVR for power quality enhancement," CPSS Transactions on Power Electronics and Applications, vol. 8, no. 4, pp. 424-436, 2023.

[4] V. Babu, K. S. Ahmed, Y. M. Shuaib, and M. Manikandan. "Power quality enhancement using dynamic voltage restorer (DVR)-based predictive space vector transformation (PSVT) with proportional resonant (PR)-controller," IEEE Access, vol. 9, pp. 155380-155392, 2021.

[5] S. S. Dheeban, and N. B. Muthu Selvan. "ANFIS-based power quality improvement by photovoltaic integrated UPQC at distribution system," IETE Journal of Research, vol. 69, no. 5, pp. 2353-2371, 2023.

[6] M. Osama abed el-Raouf, S. A. A. Mageed, M. M. Salama, M. I. Mosaad, and H. A. Abdel Hadi. "Performance enhancement of grid-connected renewable energy systems using UPFC," Energies, vol. 16, no. 11, pp. 4362, 2023.

[7] B. S. Goud, C. R. Reddy, M. Bajaj, E. E. Elattar, and S. Kamel. "Power Quality Improvement Using Distributed Power Flow Controller with BWO-Based FOPID controller," Sustainability, vol. 13, no.20, pp. 11194. 2021.

[8] N. Kanagaraj, M. Vijayakumar, M. Ramasamy, and O. Aldosari. "Energy management and power quality improvement of hybrid renewable energy generation system using coordinated control scheme," IEEE Access, 2023.

[9] W. Rohouma, M. Metry, R. S. Balog, A. A. Peerzada, M. M. Begovic, and D. Zhou. "Analysis of the capacitor-less D-STATCOM for voltage profile improvement in distribution network with high PV penetration," IEEE Open Journal of Power Electronics, vol. 3, pp. 255-270, 2022.

[10] D. Prasad, and C. Dhanamjayulu, "Solar PV-fed multilevel inverter with series compensator for power quality improvement in grid-connected systems," IEEE Access, vol. 10, pp. 81203-81219, 2022.

[11] H. Ahmed, and D. Çelik, "Enhanced upqc control scheme for power quality improvement in wave energy driven pmsg system," IEEE Transactions on Energy Conversion, 2024.

[12] M. Khaleel, Z. Yusupov, N. Yasser, H. Elkhozondar, and A. A. Ahmed. "An integrated PV farm to the unified power flow controller for electrical power system stability," Int. J. Electr. Eng. and Sustain, pp. 18-30. 2023.

[13] V. Sowmya Sree, and M. Ankarao, "Power quality enhancement of solar–wind grid connected system employing genetic-based ANFIS controller," Paladyn J. Behav. Robotics, vol. 14, no. 1, pp. 20220116, 2023.

[14] R. Adware, and V. Chandrakar. "Power quality enhancement in a wind farm connected grid with a fuzzy-based STATCOM," Engineering, Technology & Applied Science Research, vol. 13, no. 1, pp. 10021-10026, 2023.

[15] K. S. Kavin, P. Subha Karuvelam, M. Devesh Raj, and M. Sivasubramanian. "A Novel KSK Converter with Machine Learning MPPT for PV Applications," Electric Power Components and Systems, pp. 1-19, 2024.

[16] S. B. Pandu, C. K. Sundarabalan, N. S. Srinath, T. S. Krishnan, G. S. Priya, C. Balasundar, J. Sharma, G. Soundarya, P. Siano, and H. H. Alhelou. "Power quality enhancement in sensitive local distribution grid using interval type-II fuzzy logic controlled DSTATCOM," IEEE Access, vol. 9, pp. 59888-59899, 2021.

[17] J. H. Woo, L. Wu, S. M. Lee, J. B. Park, and J. H. Roh, "D-STATCOM dq axis current reference control applying DDPG algorithm in the distribution system," IEEE Access, vol. 9, pp. 145840-145851, 2021.

[18] E. Rajendran, V. Raji, and V. D. Prabu, "Power Quality Acquire of Intelligent Controller based Superior Gain Re-Lift Luo Converter Intended for PV Linked Microgrid Integration," WSEAS Transactions on Power Systems, vol. 19, pp. 1-10, 2024.

[19] Z. A. Ghafour, A. R. Ajel, N. M. Yasin, and N. M. Noaman. "Efficient Design, Analysis and Implementation of Super-Lift LUO Converter for Standalone PV Applications," Journal of Techniques, vol. 5, no. 2, pp. 81-88, 2023.

[20] P. V. V. Satyanarayana, A. Radhika, C. R. Reddy, B. Pangedaiah, L. Martirano, A. Massaccesi, A. Flah, and M. Jasiński. "Combined DC-link fed parallel-VSI-based DSTATCOM for power quality improvement of a solar DG integrated system," Electronics, vol. 12, no. 3, pp. 505, 2023.

[21] P. V. Ramana, and K. M. Rosalina. "Power Quality Enhancement Using Artificial Neural Network-Proportional Integral Controller and Fuzzy Granular Controller for DSTATCOM Integrated with Renewable Energy and Battery Storage System," Journal of New Materials for Electrochemical Systems, vol. 27, no. 4, pp. 324-339, 2024.

[22] R. Jayaraman, S. Tummapudi, R. B. R. Prakash, and T. V. Muni. "Analysis of sliding mode controller based DSTATCOM for power quality improvement in distribution power system," Materials Today: Proceedings, vol. 80, pp. 3675-3681, 2023.

[23] P. B. Patel, and S. R. Vyas. "Improving DC power supply performance: insights into Cuk and modified Cuk converters stability and power factor," Engineering Research Express, vol. 6, no. 4, pp. 045334, 2024.

[24] B. Pakkiraiah, "Solar Assisted Relift Luo Converter with UPQC for Voltage Unbalance Mitigation Using DDSRF Theory,"

[25] R. Sathyapriya, and V. Jayalakshmi, "HRES Integrated DSTATCOM Using High Gain Sepic-Zeta Based WOA Optimized ANFIS-MPPT Controller for PQ Issues," Journal of Electrical Systems, vol. 20, no. 2s, pp. 149-164, 2024.

[26] K. Nishanth, and S. Saru Krishna. "Enhancing Power Quality in Smart Grid-Connected Renewable Energy Systems Using A Hybrid Deep Learning-Based DSTATCOM: Self-Improved Jellyfish Optimizer (Si-Jo)," Optimal Control Applications and Methods, vol. 46, no. 3, pp. 912 – 936, 2025.